

# Nanoscale

Accepted Manuscript



This is an *Accepted Manuscript*, which has been through the Royal Society of Chemistry peer review process and has been accepted for publication.

*Accepted Manuscripts* are published online shortly after acceptance, before technical editing, formatting and proof reading. Using this free service, authors can make their results available to the community, in citable form, before we publish the edited article. We will replace this *Accepted Manuscript* with the edited and formatted *Advance Article* as soon as it is available.

You can find more information about *Accepted Manuscripts* in the [Information for Authors](#).

Please note that technical editing may introduce minor changes to the text and/or graphics, which may alter content. The journal's standard [Terms & Conditions](#) and the [Ethical guidelines](#) still apply. In no event shall the Royal Society of Chemistry be held responsible for any errors or omissions in this *Accepted Manuscript* or any consequences arising from the use of any information it contains.

# Chamber-Confined Silicon-Carbon Nanofiber Composites for Prolonged Cycling Life of Li-Ion Battery

Kun Fu<sup>1</sup>, Yao Lu<sup>1</sup>, Mahmut Dirican<sup>1,2</sup>, Chen Chen<sup>1</sup>, Meltem Yanilmaz<sup>1</sup>, Quan Shi<sup>1</sup>, Philip D. Bradford<sup>1</sup>, Xiangwu Zhang<sup>1\*</sup>

<sup>1</sup>*Fiber and Polymer Science Program, Department of Textile Engineering, Chemistry and Science, North Carolina State University, Raleigh, NC 27695-8301, USA*

<sup>2</sup>*Nano-Science and Nano-Engineering Program, Graduate School of Science, Engineering and Technology, Istanbul Technical University, Istanbul, 34469, TURKEY*

*\*Corresponding author. E-mail: xiangwu\_zhang@ncsu.edu*

## Abstract

Silicon is a promising high capacity (4200 mAh/g) anode material for lithium ion batteries but the significant volume change (over 300%) of silicon during lithiation/delithiation remains a challenge in terms of silicon pulverization and solid-electrolyte-interphase (SEI) accumulation in silicon composite electrode. To alleviate the volumetric change of silicon, we built a flexible and self-supporting carbon-enhanced carbon nanofiber (CNF) structure with vacant chamber to encapsulate Si nanoparticles (vacant Si@CNF@C). This composite was tested directly without any polymer and current collector. The confined vacant chamber allowed the increasing volume of silicon and SEI accumulates to be well retained for a long cycle. This chamber-confined silicon-carbon nanofiber composite exhibited an improved performance in terms of good cycling performance (620 mAh g<sup>-1</sup>), high coulombic efficiency (99%), and good capacity retention (80%) after 200 cycles. This self-supported silicon-carbon nanofiber structure showed high flexibility and good electrochemical performance for the potential as flexible electrode for lithium-ion batteries.

## 1. Introduction

To achieve high capacity and long cycle life, researchers have devoted great attentions to exploring new materials with novel structures for lithium-ion batteries.<sup>1-5</sup> Graphite, because of its capability to store one lithium for every six carbon atoms as  $\text{LiC}_6$ , has been widely used as anode with a theoretical capacity of 372 mAh/g in lithium-ion batteries. Compared with graphite, one mole of silicon (Si) can accommodate 3.75 moles of lithium and consequently has a high theoretical capacity of 3579 mAh/g at room temperature. The ten folds higher capacity of Si shows a promising potential to take the place of graphite for the next-generation lithium-ion batteries.<sup>6,7</sup>

Despite the high lithium storage capability of Si, its 300% volume change upon lithium alloying and de-alloying processes presents a major problem to the electrochemical properties and cycling performance of Si electrode. For Si particles, not only will particles undergo pulverization but also the electrode composite be detrimentally damaged due to the significant volume change of Si. The cracks and pulverizations will cause Si particles to lose electrical contacts and thus directly result in poor electrochemical performance of the electrode. In addition, solid-electrolyte-interphase (SEI) films will be formed on the fresh surface of Si after its volume expansion and surface cracking, leading to extra electrolyte consumption and electrical insulation of the electrode.

Recently, many efforts have been made to improve Si electrochemical performance by incorporating Si nanoparticles with carbon structures, including carbon coatings, graphene stacking, carbon nanotube (CNT) entanglement, and carbon nanofiber (CNF) confinement.<sup>8-11</sup> It has been well demonstrated that the electrochemical performance of

Si-based electrodes can be greatly improved by employing a proper spatial correlated carbon matrix.<sup>12</sup> Since the facile synthesis and flexible design of CNFs, especially for electrospun polyacrylonitrile (PAN)-derived carbon nanofibers, the composite of CNFs and Si (CNF-Si) attracts considerable attentions for the development of long cycling life and high capacity of Si composite electrode. As an important component of Si composite electrodes, CNFs outperform other carbon structures in three key characteristics: (a) high lithium storage capacity, (b) self-constructed flexible structure, and (c) good electrolyte retention. Thus, designing an empty space to accommodate the Si volume expansion within CNFs becomes important for the improvement of the cycle performance.<sup>7,13-15</sup> Recently, Cui and co-workers introduced engineered empty space around silicon nanoparticles, which was able to accommodate the Si volume change and resulted in high cycling stability of Si.<sup>13</sup> In that work, silica was first utilized as a sacrificial material to wrap the Si nanoparticles and it was then removed by hydrofluoric acid (HF) to create the vacant space after CNFs were formed. By encapsulating Si into the empty space of CNFs, the resultant anode reached a capacity of  $> 800 \text{ mAh g}^{-1}$ , a coulombic efficiency of  $> 99\%$ , and a capacity retention of  $\sim 90\%$  after 200 cycles. Inspired by this work, Guo and co-workers reported a porous Si@CNF composite, which was prepared by electrospinning Si@SiO<sub>2</sub> into CNFs followed by HF etching. The resultant electrode delivered a capacity of  $\sim 1100 \text{ mAh g}^{-1}$ , a coulombic efficiency of  $> 97\%$ , and a capacity retention of  $\sim 69\%$  after 100 cycles.<sup>15</sup> The relatively low coulombic efficiency and low capacity retention of the porous Si@CNF composite indicates that the porous CNF structure alone was not sufficient in accommodating the Si volume change and further

improvement is needed to *simultaneously* achieve the high capacity and good cycling stability for the porous Si@CNF structure.

In this communication, we applied additional carbon coating to the porous Si@CNF structure to enhance the chamber structure around Si nanoparticles within the CNF structure. The designed vacant Si@CNF@C composite has a flexible and self-supporting structure prepared by electrospinning and chemical vapor deposition (CVD) techniques. The electrode can be used directly as a binder-free anode in lithium-ion batteries. The enhanced vacant space was designed to accommodate the increasing volume of Si and SEI formed during lithium insertion while containing pulverized Si to minimize the dramatic capacity loss of the electrode.<sup>16</sup> The carbon coating can make up for the defects of CNFs caused by the HF etching process and help encapsulate Si completely within the CNF structure so as to localize the pulverized Si over a long cycle life. The novelty of this work is that it utilizes the synergetic effects of vacant space and CVD carbon coating to achieve good electrochemical performance for Si-containing electrodes. Results demonstrated that by encapsulating Si nanoparticles in a carbon coating-enhanced chamber structure of CNF, the resultant vacant Si@CNF@C electrode exhibited good cycling performance in terms of high capacity (620 mAh g<sup>-1</sup>), high coulombic efficiency (99%), and good capacity retention (80%) after 200 cycles.

## 2. Experimental

### 2.1. Preparation of Si@SiO<sub>2</sub>

200 mg Si nanoparticles (30-50 nm, Nanostructured & Amorphous Materials) were dispersed in a mixture solution of 350 mL ethanol and 100 mL water. After 1 hour sonication, 5 mL ammonium hydroxide was dropped into the solution with vigorous

stirring. Then 3.5 g tetraethoxysilane (TEOS, Aldrich) was dropped into the solution with mechanical stirring and kept at room temperature overnight. After centrifugation and washing with DI water, the as-prepared Si@SiO<sub>2</sub> particles were dried in vacuum oven for 12 hours.

## **2.2. Fabrication of vacant Si@CNF@C composites**

Polyacrylonitrile (PAN) (M<sub>w</sub> = 150,000 g/mol, Aldrich) was used as the carbon precursor for the CNFs. Si@SiO<sub>2</sub> (10 wt.%) was dispersed in an 8 wt.% PAN solution in DMF. The as-prepared dispersion was then electrospun into Si@PAN nanofibers with a flow rate of 0.75 ml/h at 1.5 kV. The as-prepared nanofibers were stabilized in air at 280 °C for 5.5 hours (heating rate: 5 °C min<sup>-1</sup>) and then carbonized at 760 °C in argon for 1 hour (heating rate: 2 °C min<sup>-1</sup>) to obtain the Si@SiO<sub>2</sub>@CNF composite mat. The nanofiber composite was then coated with carbon via CVD through the thermal decomposition of acetylene (C<sub>2</sub>H<sub>2</sub>) as the carbon precursor gas. The deposition occurred at 760 °C, 600 sccm flow rate of acetylene while the system was maintained at 20 torr for 30 min. These conditions allowed for a relatively slow but uniform deposition of carbon on the nanofiber surface. The as-prepared nanofibers were then soaked in 10 wt.% hydrofluoric acid (HF) aqueous solution for 5 hours to remove the SiO<sub>2</sub>. After cleaning in DI water and drying in an oven, the vacant Si@CNF@C composite was obtained. For comparison, solid Si@CNF and vacant Si@CNF composite mats were also prepared.

## **2.3. Characterizations**

The morphology of nanofibers was investigated using a field emission scanning electron microscopy (FE-SEM, JEOL 6400F) and transmission electron microscope (TEM, HITACHI HF2000, accelerating voltage 200 kV) equipped with selected area electron

diffraction (SAED). The crystallographic and chemical structures were studied using wide angle X-ray diffraction (WAXD, Rigaku Smartlab) and a Renishaw Raman microscope (514 nm).

#### 2.4. Electrochemical Evaluations

The vacant Si@CNF@C nanofibers formed a conductive, free-standing mat that was punched directly into binder-free disk-like electrodes with 0.5 inch in diameter. The counter electrode used was lithium ribbon (99.9%, Aldrich). The electrolyte used was 1 M LiPF<sub>6</sub>/ethylene carbonate (EC) + dimethyl carbonate (DMC) + diethyl carbonate (DEC) (1:1:1 by volume, MTI Corporation). The 2032 coin cells were assembled in a high-purity argon-filled glove box. All cells were tested with cut-off potentials of 0.01 and 2.0 V using a LAND-CT 2001A battery test system. The coulombic efficiency was calculated as the ratio of the capacity for Li insertion to the capacity for the Li extraction.

### 3. Results and Discussions

The procedure for synthesizing the vacant Si@CNF@C composite is shown in **Figure 1**. Tetraethoxysilane (TEOS) as silicon dioxide (SiO<sub>2</sub>) precursor was used to grow silica coatings on Si nanoparticles.<sup>17</sup> The as-prepared SiO<sub>2</sub>-coated Si (Si@SiO<sub>2</sub>) nanoparticles were electrospun into polyacrylonitrile (PAN) nanofibers followed by carbonization (760 °C) to obtain Si@SiO<sub>2</sub> nanoparticle-filled carbon nanofiber (Si@SiO<sub>2</sub>@CNF) mat. The as-prepared nonwoven mat was then coated by amorphous carbon via CVD technique to obtain Si@SiO<sub>2</sub>@CNF@C. During the CVD coating, the carbon precursor, acetylene (C<sub>2</sub>H<sub>2</sub>) gas, was introduced with a flow rate of 600 sccm at 760 °C for 30 min. After the CVD coating process, any Si particles that were initially exposed on the fiber surface

were completely coated with carbon.<sup>16</sup> The confined vacant space was created after removing SiO<sub>2</sub> through exposure to hydrofluoric (HF) acid. After cleaning with deionized water and drying in oven, the vacant Si@CNF@C composite nonwoven mat was ready for electrochemical testing.

**Figure 2** shows the morphological characterization of the vacant Si@CNF@C composite. For comparison, a TEM image of Si@SiO<sub>2</sub> nanoparticles is shown in Figure 2a. It is seen that the as-prepared Si@SiO<sub>2</sub> nanoparticles exhibit a clear core-shell structure. Diameters of the as-prepared Si@SiO<sub>2</sub> nanoparticles were around 100 - 200 nm, in comparison with the 30 - 100 nm diameter of pristine Si nanoparticles. Vacant space can be observed clearly after removing the SiO<sub>2</sub> coating from the nanoparticles embedded in the CNF matrix (Figure 2b). Due to the agglomeration of Si@SiO<sub>2</sub> nanoparticles, a continuous tunnel-like vacant space was created within the CNFs encapsulating the Si particles. The size of the vacant space can be manipulated by adjusting the thickness of SiO<sub>2</sub> coating through TEOS treatment. Here, the size of vacant space created is larger than the size of pristine Si nanoparticles, which can provide sufficient space to accommodate silicon's 300% volume expansion. In a previous study, it was found that nanoparticles are often attached to or partially embedded in the carbon nanofibers to form Si clusters, which can deteriorate the carbon matrix during Si volume expansion leading to structural failure of the fibers and rapid capacity loss.<sup>12</sup> In this work, the amount of Si@SiO<sub>2</sub> nanoparticles, the thickness of SiO<sub>2</sub> coating and the thickness of CVD carbon coating were controlled to obtain a good vacant Si@CNF@C structure as shown in Figures 2c and 2d. This self-supported and binder-free composite shows good flexibility as shown in Figure 2e. It can endure several cycles of bending test without obvious fracture. The nonwoven mat can be

used as an electrode directly without current collector or polymer binder. This structure can be promisingly applied to the flexible batteries. In the battery testing, the nonwoven Si@CNF@C composite were cut directly into disks fitting for the 2032 coin-type cells (Figure 2f). The average mass of the electrode used in this work was  $1.43 \text{ mg/cm}^2$ .

The characterization of Si@SiO<sub>2</sub> nanoparticles as well as their corresponding composites was carried out using Fourier transform infrared (FT-IR) spectroscopy, Raman spectroscopy, and X-ray diffraction (XRD) techniques (**Figure 3**). In the FT-IR spectrum of Si@SiO<sub>2</sub> nanoparticles (Figure 3a), the SiO<sub>2</sub> coating can be confirmed by the characteristic peaks of bending and stretching of Si-O-Si bonds at 798 and 1081 cm<sup>-1</sup>, respectively.<sup>18</sup> The small shoulder at 1200 cm<sup>-1</sup> is related to different vibration mode of SiO<sub>2</sub>.<sup>19</sup> The peaks at 950 and 1632 cm<sup>-1</sup> come from the residual of TEOS.<sup>19</sup> Si@SiO<sub>2</sub> nanoparticles were further analyzed by Raman spectroscopy as shown in Figure 3b. As control, pristine Si nanoparticles were examined and they showed a sharp peak of around 520 cm<sup>-1</sup>, indicating the crystalline nature of Si.<sup>20</sup> For the Si@SiO<sub>2</sub> nanoparticles, a characteristic peak of the D<sub>1</sub> defect from sol-gel derived silica (SiO<sub>2</sub>) was detected at around 500 cm<sup>-1</sup>, confirming the presence of SiO<sub>2</sub> coating on the Si surface.<sup>21</sup> After incorporation into the CNF matrix and coated with CVD carbon, the Raman spectra of the resultant vacant Si@CNF@C composite as well as Si@SiO<sub>2</sub>@CNF@C composite (before HF etch) are shown in Figure 3c. Both Si and SiO<sub>2</sub> were detected before HF etching. After HF etching, only the crystalline Si peak was present, indicating the complete removal of SiO<sub>2</sub> coating. In Figure 3d, the Raman spectrum (carbon) of the vacant Si@CNF@C composite exhibited a high *R*-value (>1), which is the ratio of *D* band (1340 cm<sup>-1</sup>) intensity to the *G* band (1580 cm<sup>-1</sup>) intensity, indicating the disordered

structure of the CNF matrix and CVD carbon coating. The disordered carbon and crystalline Si structures of the vacant Si@CNF@C were also confirmed by the XRD spectrum in Figure 3e.

Electrochemical properties of the vacant Si@CNF@C composite were tested in 2032 coin cells by using lithium metal foil as the counter electrode for charging and discharging in the voltage range of 0.01 - 2 V vs. Li<sup>+</sup>/Li at 100 mA h<sup>-1</sup>. The results of this testing are shown in **Figure 4**. For comparison, traditional binder-assisted Si electrode was tested as the control (Figure 4a). It was prepared by mixing Si nanoparticles with polyvinylidene fluoride (PVdF) polymer binder and carbon black (8:1:1 by weight). The PVdF-assisted Si electrode had charge and discharge capacity of 873 and 3264 mAh g<sup>-1</sup>, respectively, with a low coulombic efficiency (CE) of 27%, at the first cycle. At the 5<sup>th</sup> cycle, charge capacity dropped rapidly to 400 mAh g<sup>-1</sup> with almost 54% capacity loss. This is a common phenomenon for PVdF binder-assisted Si electrodes. The PVdF polymer cannot effectively hold Si and carbon additives together, thus leading to the loss of mechanical and electronic connections.<sup>22</sup> In addition, the ionic conductivity of Si will be negatively influenced by the polymer coating on surface. Thus, binder-free structure provides the opportunity to solve the concerns related to mechanical adhesion, electronic connection, and ionic retention existing in the conventional binder system of Si electrodes. Confining Si nanoparticles in the CNF matrix can provide an effective way to address those challenges seen in binder-assisted Si electrodes. In addition to the vacant Si@CNF@C composite electrode, other forms of CNF-based electrodes, *i.e.*, solid Si@CNF (composite with pristine Si nanoparticles) and vacant Si@CNF (composite by removing SiO<sub>2</sub> from Si@SiO<sub>2</sub>@CNF without CVD carbon coating), were also

synthesized and tested. The specific capacities for these composite electrodes were calculated based on the total mass of Si, CNF, and carbon coating if any. The solid Si@CNF composite exhibited charge and discharge capacities of 855 and 1302 mAh g<sup>-1</sup>, respectively, with a CE of 66% through the first cycle (Figure 4b). The charge capacity decreased to 738 mAh g<sup>-1</sup> with a 16% capacity loss at the 5<sup>th</sup> cycle. In the solid Si@CNF composite, CNF cannot be sufficiently confine the nanoparticles by providing a buffer zone for the expansion of the Si. For the vacant Si@CNF composite, the initial charge and discharge capacities reached 977 and 1890 mAh g<sup>-1</sup>, respectively, with a CE of 51.7% (Figure 4c). High irreversible capacity was observed in the 2<sup>nd</sup> lithiation process, indicating that excessive electrolyte was consumed due to the formation of heavy SEI. At the 5<sup>th</sup> cycle, charge capacity was remained at 598 mAh g<sup>-1</sup>, with a capacity loss of 39%. This dramatic capacity loss can be ascribed to the detachment of Si nanoparticles from the opening of porous CNF matrix during Si volume expansion and extraction process. This can be attributed to the large number of particles that reside on the fiber surface after spinning and carbonization. Among all electrodes studied, the vacant Si@CNF@C composite demonstrated the best charge-discharge properties (Figure 4d). Its initial charge and discharge capacities were 780 and 1328 mAh g<sup>-1</sup>, respectively, with a CE of 58.7%. As compared to the vacant Si@CNF composite without CVD carbon coating, the area under the curve of electrolyte reduction/degradation stage (~0.7V) became smaller for the vacant Si@CNF@C composite, indicating that less electrolyte participated in the formation of SEI. At the 5<sup>th</sup> cycle, vacant Si@CNF@C composite exhibited a capacity retention of 81% retention with a capacity value of 632 mAh g<sup>-1</sup>, which was the highest among all electrodes studied.

The cycling performance and coulombic efficiencies are shown in Figures 4e and 4f, respectively. The binder-assisted Si electrode showed rapid capacity decay and its charge capacity was only 153 mAh g<sup>-1</sup> at the 50<sup>th</sup> cycle, which is not acceptable for the long cycle life requirement of practical batteries. For comparison, the performance of pure carbon nanofibers is also shown. Results showed that pure carbon nanofibers exhibited a higher charge capacity of 300 mAh g<sup>-1</sup> at 50<sup>th</sup> cycle, which is still not satisfactory. It is also seen that both electrodes showed large variations in the coulombic efficiencies during the cycling. For solid Si@CNF, vacant Si@CNF, and vacant Si@CNF@C composites, they exhibited different cycle behaviors in 200 cycles. The capacity of solid Si@CNF declined to 216 mAh g<sup>-1</sup> at the 200<sup>th</sup> cycle, with a capacity retention of 25%. The corresponding coulombic efficiency increased from 65.6% to 98.0% in the beginning 13 cycles, followed by an apparent decrease to 95.8% at around 40<sup>th</sup> cycle. After that, the coulombic efficiency increased again and eventually maintained at 99.0% in the following cycles. The dramatic coulombic efficiency change of solid Si@CNF can be ascribed to the volume change of Si nanoparticles during cycling. In addition, a small *bump* occurred in the cycling curve of solid Si@CNF composite, which is correlated to the *bowl* shape of CE curve in the first 50 cycles. Such correlated capacity and coulombic efficiency changes may be the result of the lithiation delay of the embedded Si compared with the attached Si on the CNF as well as the detachment of Si from the CNFs.<sup>12</sup> For the vacant Si@CNF composite, the cycling curve exhibited a fast capacity loss trend. The charge capacity decreased from 978 to 414 to 320 mAh g<sup>-1</sup> at 50<sup>th</sup> and 200<sup>th</sup> cycle, respectively. The corresponding CE value increased from 52% to 99% quickly in the first 10 cycles and maintained above 99.5% in the following cycles. The short time needed to

achieve high CE value (>99%) indicates that porous CNF could facilitate the contact between Si and electrolyte and eliminate the lithiation delay of embedded Si caused by the blocking effect of CNF matrix. However, due to the lack of protection to Si, the Si nanoparticle detachment significantly reduced the capacity and there were only 51%, 42%, and 32% capacity retained at 10<sup>th</sup>, 50<sup>th</sup>, and 200<sup>th</sup> cycle, respectively. Along with heavy SEI growth in the electrode, the vacant Si@CNF composite suffered severely structural failure and fast capacity fading. The carbon coating that was applied as the final layer on the vacant Si@CNF@C composite was designed to address those issues.

After the CVD carbon coating, the vacant Si@CNF@C composite showed a significant improvement in the cyclic stability, coulombic efficiency (>99%), and capacity retention (80%), demonstrating the enhanced confinement of Si nanoparticles in the empty chamber. As shown in Figure 4e, the capacity decreased from 780 to 612 mAh g<sup>-1</sup> in the first several cycles, and then it kept increasing to 784 mAh g<sup>-1</sup> until the 85<sup>th</sup> cycle. After that, the capacity only experienced a slight decrease and a relatively high capacity of 620 mAh g<sup>-1</sup> was achieved at the 200<sup>th</sup> cycle. Correspondingly, the CE curve of vacant Si@CNF@C showed a different trend compared with that of vacant Si@CNF composite. The CE increased from 58.7% at the 1<sup>st</sup> cycle to 99.2% at the 12<sup>th</sup> cycle and it remained above 99% until 99.7% at the 51<sup>st</sup> cycle. Then, the CE value decreased slightly to 98.5% at the 95<sup>th</sup> cycle and kept increasing to 99.9% in the following 100 cycles. It took only several cycles for the vacant Si@CNF@C composite to achieve a high CE value (>99%), which was similar to the vacant Si@CNF. This further confirms that porous CNF provides direct contact between Si and electrolyte in the confined vacant space. During cycling, along with the increase in capacity in the first 85 cycles, it is observed that the

CE value decreased slightly, following by a continuous increase. The phenomenon that the capacity increased first and then decreased was only observed for the vacant Si@CNF@C composite. Similar behavior has been found in different Si-carbon core-shell structure materials,<sup>8,13,14</sup> but few researchers have given attention to the capacity increase during cycling. For the vacant Si@CNF@C composite, this unique phenomenon can be explained by the fact that Si nanoparticles were fully preserved within the chamber of CNF even if they suffered large volume expansion and pulverization, which avoided the the damage of the composite structure. For those pulverized Si particles within the well confined chambers, smaller particle size would enable shorter lithium transfer distance, which facilitated Si to be further activated and led to increased capacity. However, when the cycle number was greater than 100, the limited chamber space was eventually filled up by the pulverized Si and SEI products and was no longer able to accomodate the volume change, leading to decreased capacity. On the other hand, for the solid Si@CNF structure, the volume change of Si would break the CNF structure in the first few cycles, causing Si nanoparticles to continuously separate from the CNFs with each additional cycle, which in turn resulted in fast capacity decay.<sup>12</sup> Therefore, the capacity increase phenomenon was only observed for the vacant Si@CNF@C structure.

Although some researchers have used *in-situ* methods to observe the lithiation of Si as well as its composites,<sup>12,23,24</sup> it is still challenging to examine the structural evolution of vacant Si@CNF@C composite in the long range of battery cycling. In this work, we disassembled batteries after cycling to observe the morphology change of the Si composite using TEM. Prior to TEM observation, the cycled electrode was washed by HCl to remove SEI. **Figure 5a** shows the vacant Si@CNF@C structure before cycling. The

confined vacant space as well as Si can be clearly observed. After cycling, the CNF suffered damages and the resultant morphology is dependent on the cycle number. **Figure 5b** shows a representative image of what the structure of vacant Si@CNF@C looked like after 100 cycles. The entire vacant space of CNF was occupied with opaque substances. These substances may have been the pulverized Si and decomposed electrolyte. This was probably due to the continuous SEI growth accompanied with Si pulverization that gradually took up the whole space. When the vacant holes have no remaining space to accommodate the SEI growth and Si pulverization, the new generated SEI and pulverized Si will eventually break the thin carbon walls and destroy the vacant CNF structure as shown in **Figure 5c**. After 200 cycles, the CNF matrix was severely damaged, therefore capacity kept decreasing. The schematic interpretation of this process is shown in **Figure 5d** to describe the Si evolution in the vacant Si@CNF@C structure. In the first lithiation process, large SEI was formed on both outer and inner surfaces of the carbon fibers (ii). During cycling, the pulverization of Si resulted in more surface area for SEI formation. After prolonged cycling, the carbon chamber was filled up with SEI and pulverized Li-Si and the filling material began to expand the CNF (iii). Eventually, continuous SEI growth as well as the expansion of Si broke the carbon chamber and the pulverized Si would expose to the electrolyte directly with no carbon protection (iv). According to these observations and analyses, we have to admit that, eventually, capacity decreasing and carbon chamber breaking are inevitable due to the continuous SEI growth. Therefore, the key for the design of the spatial-related Si-carbon nanofiber composite is to avoid Si agglomeration and achieve the complete encapsulation of Si in carbon nanofibers, then to design large enough chamber to accommodate the 300% volume

expansion of Si and the increasing growth of SEI, so as to postpone SEI production exceeding the limited volume of empty space and realize the long cycling life and high capacity.

#### 4. Conclusions

In summary, we have successfully designed and fabricated composite anodes of CNFs with confined vacant spaces containing Si nanoparticles. This material is a flexible and binder-free electrode produced by electrospinning and CVD techniques. Compared to other forms of Si@CNF composites, the resultant vacant Si@CNF@C exhibited excellent properties in terms of cycle performance (620 mAh g<sup>-1</sup> at 200th cycle), coulombic efficiency (99%), and capacity retention (80%) in 200 cycles. The confined vacant space can accommodate the huge volume expansion of Si and the formation of SEI while preserving the pulverized nanoparticles to prevent dramatic capacity loss and extend the Si cycle life for hundreds of cycles. This design can be also extended to other materials suffering from large volume change issues during energy storage.

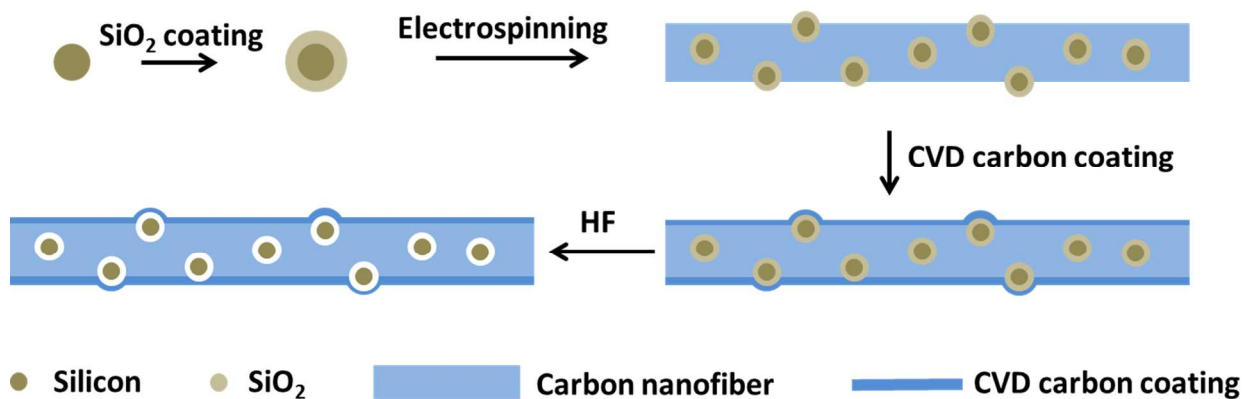
#### ACKNOWLEDGEMENTS

This work was supported by the U.S. Department of Energy under grant no: DE-EE0001177, Advanced Transportation Energy Center, and ERC Program of the National Science Foundation under Award Number EEC-08212121. The authors acknowledge the use of the Analytical Instrumentation Facility (AIF) at North Carolina State University, which is supported by the State of North Carolina and the National Science Foundation. The authors also thank Dr. Yuntian Zhu for the use of Raman microscope.

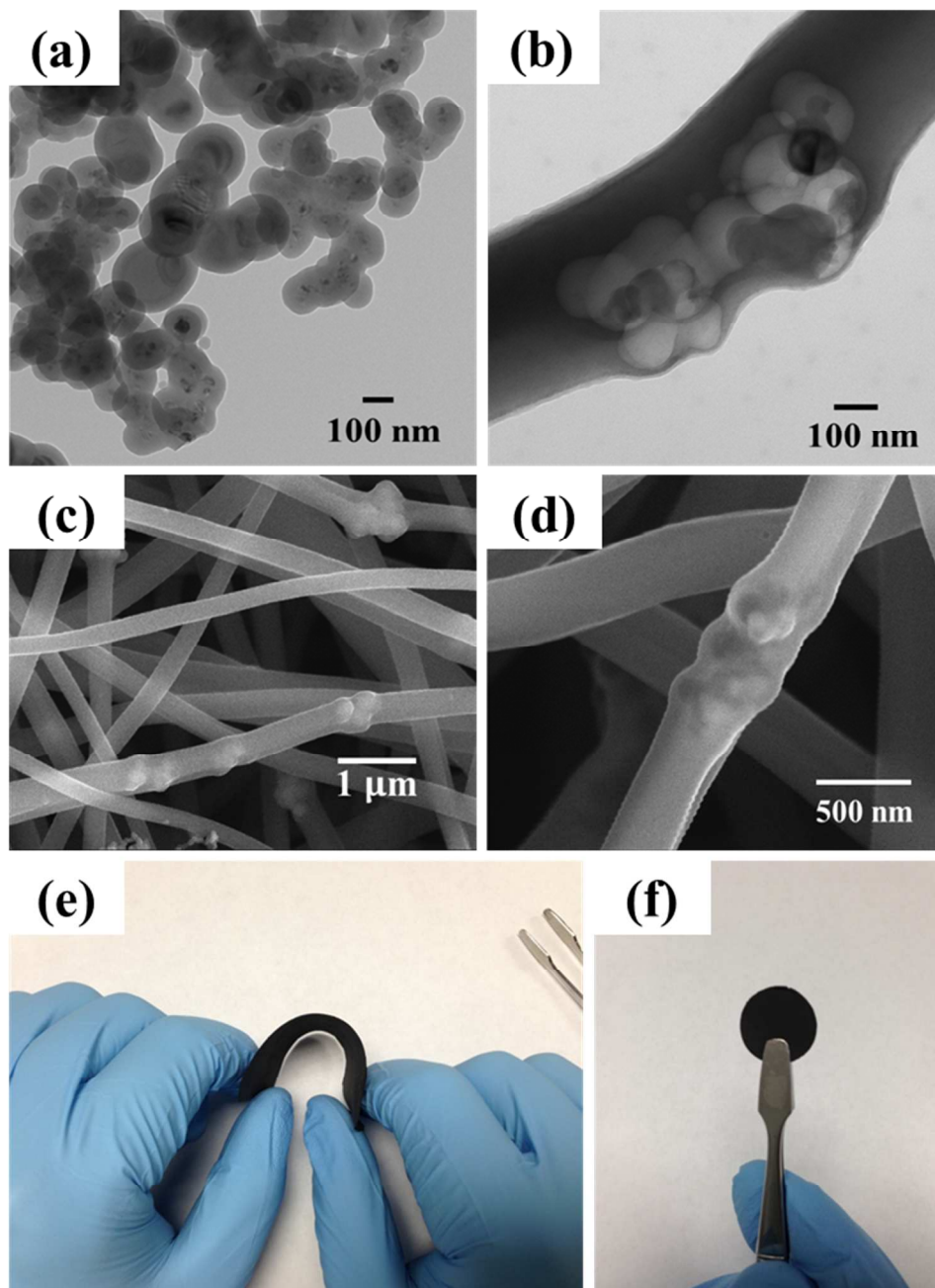
## REFERENCES

1. T.-H. Kim, J.-S. Park, S. K. Chang, S. Choi, J. H. Ryu, and H.-K. Song, *Adv. Energy Mater.*, 2012, **2**, 860–872.
2. P. G. Bruce, B. Scrosati, and J.-M. Tarascon, *Angew. Chem. Int. Ed.*, 2008, **47**, 2930–2946.
3. L. Ji, Z. Lin, M. Alcoutlabi, and X. Zhang, *Energy Environ. Sci.*, 2011, **4**, 2682–2699.
4. S. Xin, Y.-G. Guo, and L.-J. Wan, *Acc. Chem. Res.*, 2012, **45**, 1759–1769.
5. J. B. Goodenough and Y. Kim, *Chem. Mater.*, 2010, **22**, 587–603.
6. J. Dahn and T. Zheng, *Sci. ...*, 1995, **270**, 590–593.
7. T. H. Hwang, Y. M. Lee, B.-S. Kong, J.-S. Seo, and J. W. Choi, *Nano Lett.*, 2012, **12**, 802–807.
8. N. Liu, H. Wu, M. T. McDowell, Y. Yao, C. Wang, and Y. Cui, *Nano Lett.*, 2012, **12**, 3315–3321.
9. B. Wang, X. Li, X. Zhang, B. Luo, M. Jin, M. Liang, S. a Dayeh, S. T. Picraux, and L. Zhi, *ACS Nano*, 2013, **7**, 1437–1445.
10. L. Ji and X. Zhang, *Carbon N. Y.*, 2009, **47**, 3219–3226.
11. K. Fu, O. Yildiz, H. Bhanushali, Y. Wang, K. Stano, L. Xue, X. Zhang, and P. D. Bradford, *Adv. Mater.*, 2013, **25**, 5109–5114.
12. M. Gu, Y. Li, X. Li, S. Hu, X. Zhang, W. Xu, S. Thevuthasan, D. R. Baer, J.-G. Zhang, J. Liu, and C. Wang, *ACS Nano*, 2012, **6**, 8439–8447.
13. H. Wu, G. Zheng, N. Liu, T. J. Carney, Y. Yang, and Y. Cui, *Nano Lett.*, 2012, **12**, 904–909.
14. H. Wu, G. Chan, J. W. Choi, I. Ryu, Y. Yao, M. T. McDowell, S. W. Lee, A. Jackson, Y. Yang, L. Hu, and Y. Cui, *Nat. Nanotechnol.*, 2012, **7**, 310–315.
15. X. Zhou, L.-J. Wan, and Y.-G. Guo, *Small*, 2013, 1–5.
16. K. Fu, L. Xue, O. Yildiz, S. Li, H. Lee, Y. Li, G. Xu, L. Zhou, P. D. Bradford, and X. Zhang, *Nano Energy*, 2013, **2**, 976–986.

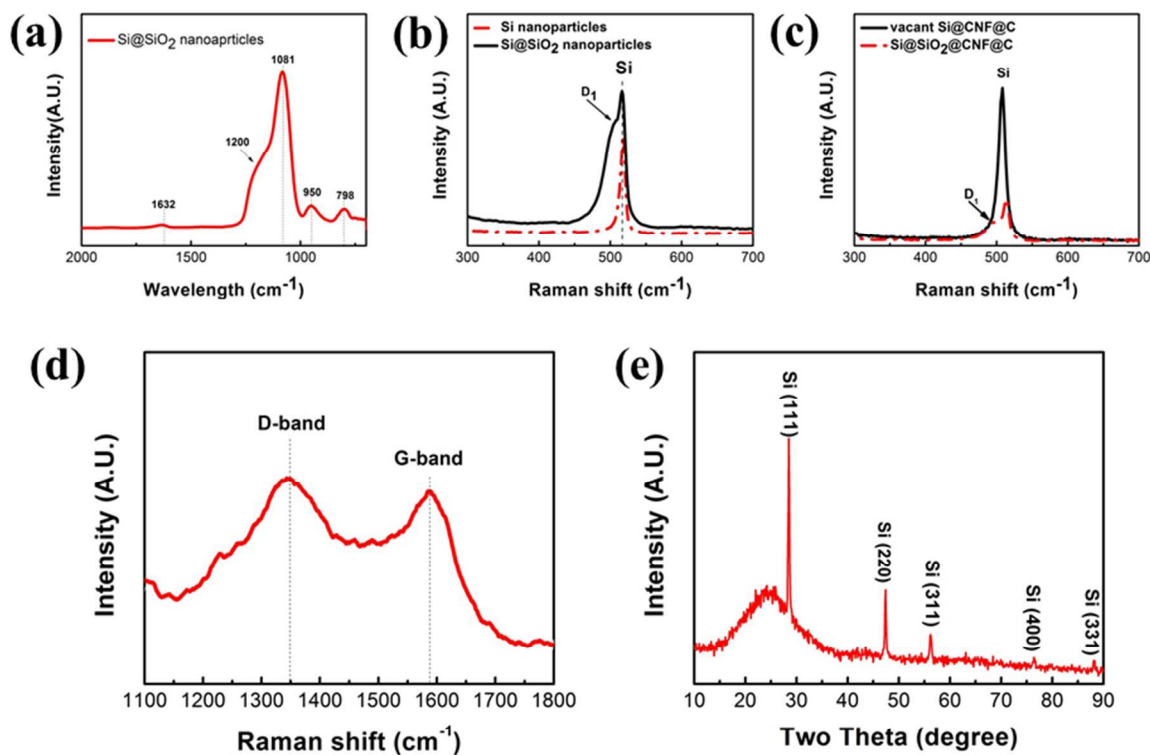
17. J. Zhang, P. Zhan, Z. L. Wang, W. Y. Zhang, and N. B. Ming, *J. Mater. Res.*, 2003, **18**, 649–653.
18. B. Shokri, M. Firouzjah, and S. Hosseini, in *IPCS-Conference*, 2009, pp. 1–4.
19. G. Katumba, J. Lu, L. Olumekor, G. Westin, and E. Wäckelgård, *J. Sol-Gel Sci. Technol.*, 2005, **36**, 33–43.
20. A. T. Voutsas, M. K. Hatalis, J. Boyce, and A. Chiang, *J. Appl. Phys.*, 1995, **78**, 6999–7006.
21. C. J. Brinker, D. R. Tallant, E. P. Roth, and C. S. Ashley, in *MRS Proceedings*, 1985, vol. 61, pp. 387–411.
22. M. Wu, X. Xiao, N. Vukmirovic, S. Xun, P. K. Das, X. Song, P. Olalde-Velasco, D. Wang, A. Z. Weber, L.-W. Wang, V. S. Battaglia, W. Yang, and G. Liu, *J. Am. Chem. Soc.*, 2013, **135**, 12048–12056.
23. M. T. McDowell, S. W. Lee, J. T. Harris, B. A. Korgel, C. Wang, W. D. Nix, and Y. Cui, *Nano Lett.*, 2013, **13**, 758–64.
24. J.-S. Bridel, T. Azai<sup>□</sup>s, M. Morcrette, J.-M. Tarascon, and D. Larcher, *J. Electrochem. Soc.*, 2011, **158**, A750–A759.



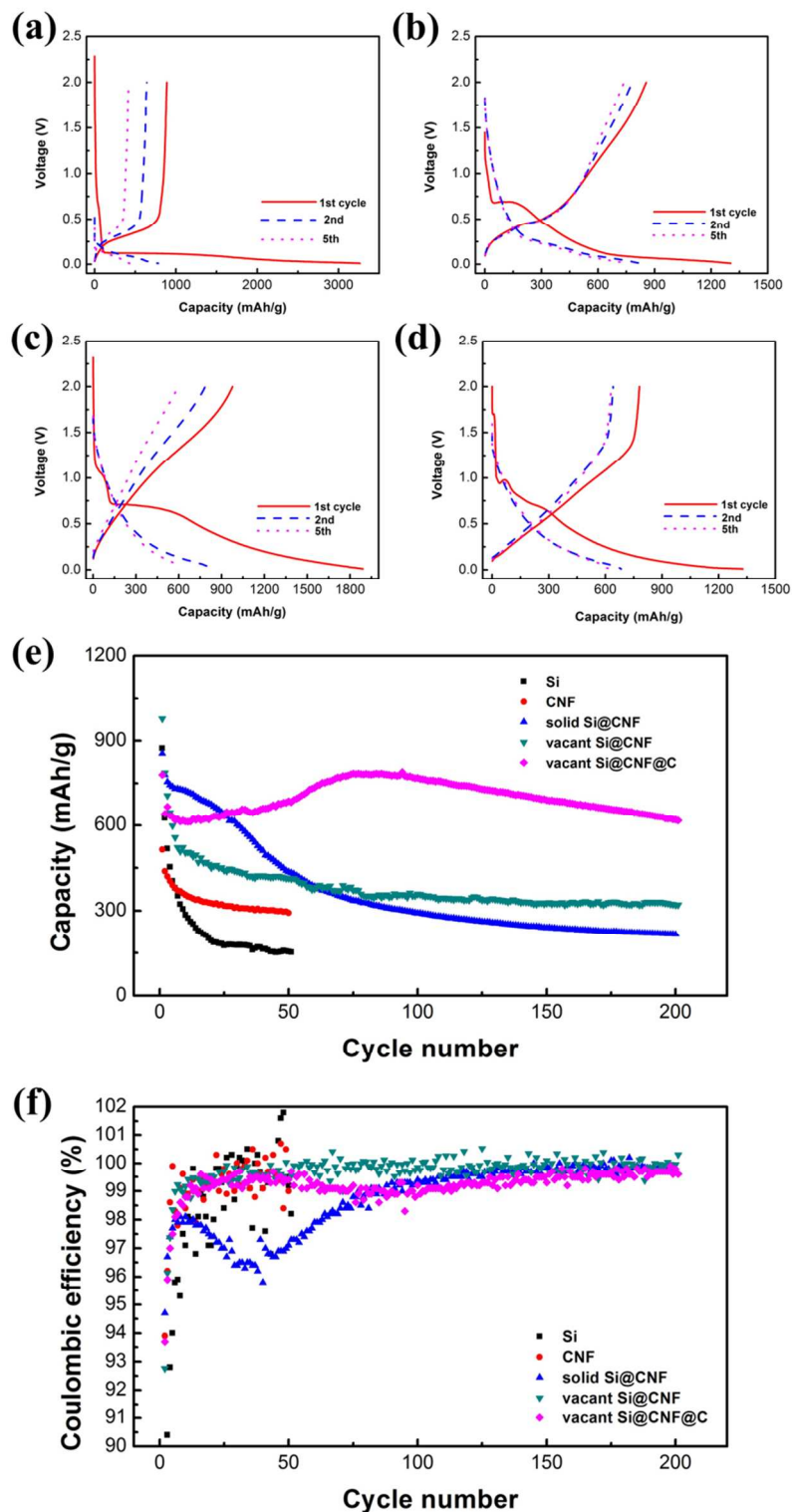
**Figure 1. Schematic design of vacant Si@CNF@C composite.** SiO<sub>2</sub> was coated on Si nanoparticles by hydrolysis of TEOS. The as-prepared Si@SiO<sub>2</sub> nanoparticles were electrospun into PAN nanofibers followed by carbonization and CVD carbon coating. After removing the SiO<sub>2</sub> with HF acid, confined vacant spaces were created for the Si nanoparticles.



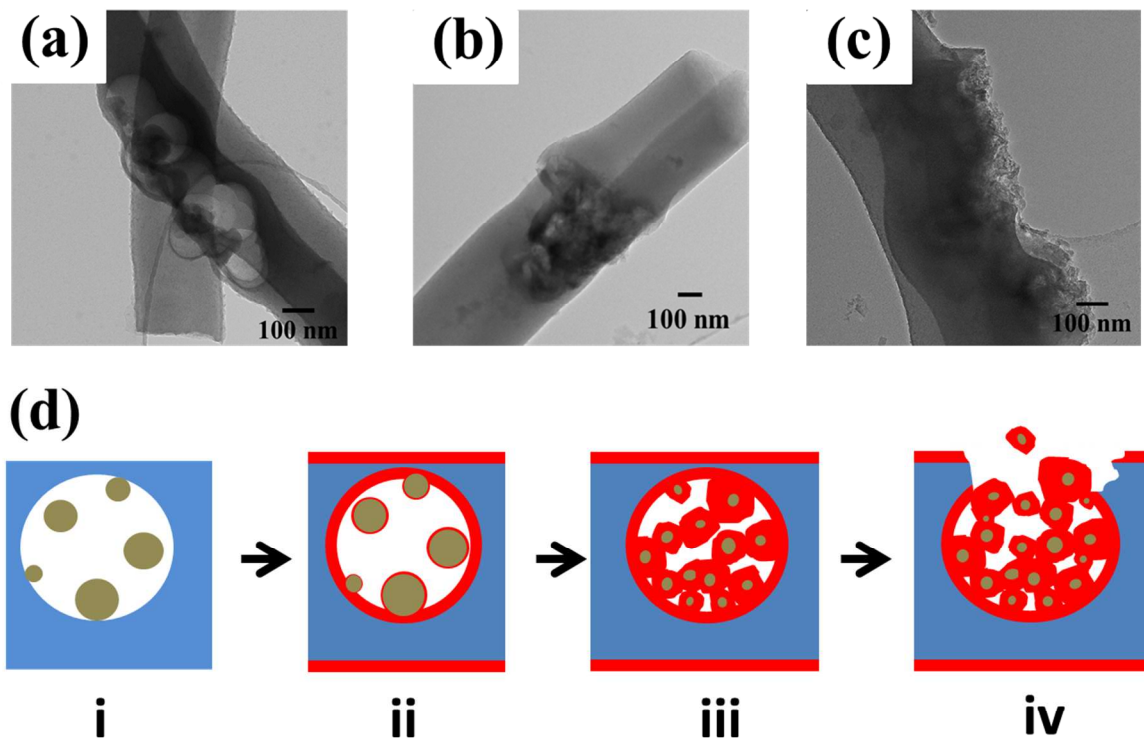
**Figure 2. Morphological characterization of vacant Si@CNF@C composite.** (a) TEM image of Si@SiO<sub>2</sub> nanoparticles. (b) TEM image of a vacant Si@CNF@C nanofiber. (c-d) SEM images of a vacant Si@CNF@C nanofiber mat with low and high magnifications. (e) Photograph showing excellent flexibility of the vacant Si@CNF@C nanofiber mat. (f) As-punched disk as a binder-free electrode for coin-type lithium-ion cell.



**Figure 3. Characterizations of Si@SiO<sub>2</sub> nanoparticles and vacant Si@CNF@C composite.** (a) FT-IR spectrum of Si@SiO<sub>2</sub> nanoparticles. (b) Raman spectra (Silicon) of Si and Si@SiO<sub>2</sub> nanoparticles. SiO<sub>2</sub> was grown on Si surface. (c) Raman spectra (Silicon) of Si@SiO<sub>2</sub>@CNF@C composite and vacant Si@CNF@C composite. (d) Raman spectrum (Carbon) of vacant Si@CNF@C composite. D-band peak is higher than G-band peak, indicating the amorphous structure of carbon-coated CNF. (e) XRD pattern of vacant Si@CNF@C composite.

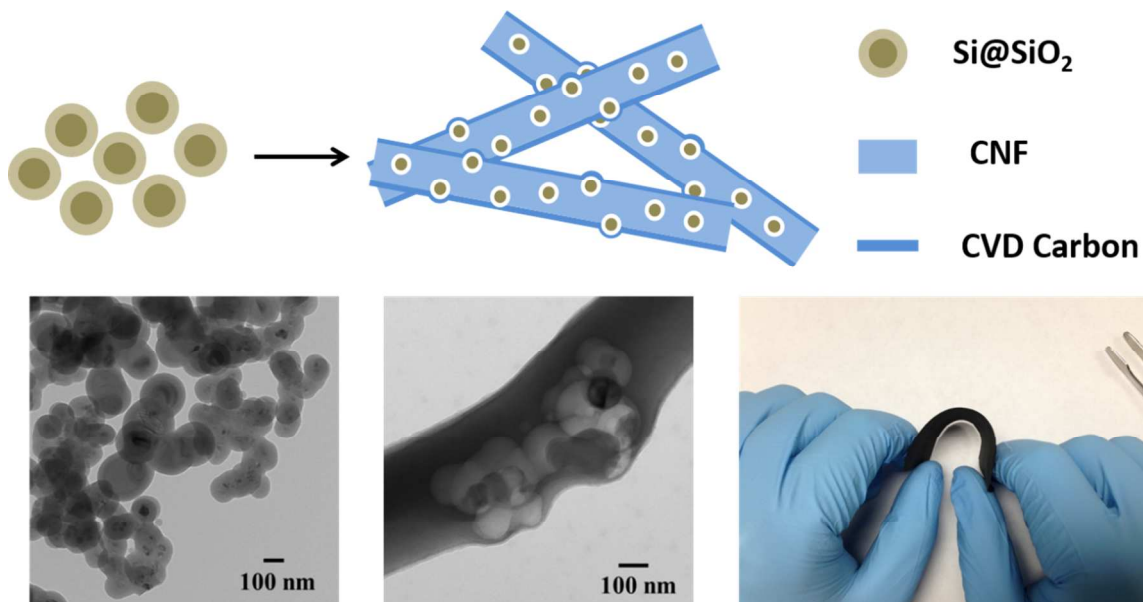


**Figure 4. Electrochemical characterization of various types of Si and CNF composites.** Galvanostatic charge-discharge profile of (a) PVdF-assisted Si electrode, (b) solid Si@CNF, (c) vacant Si@CNF, and (d) vacant Si@CNF@C composites. (e) Cycle performance and (f) coulombic efficiencies of different types of Si nanoparticle-based electrodes.



**Figure 5. Electrode morphology before and after electrochemical cycling.** TEM images of (a) pristine vacant Si@CNF@C electrode and cycled electrodes after (b) 100 cycles and (c) 200 cycles. (d) Schematic of Si evolution in the Si@CNF@C electrode: i. silicon nanoparticles are in the empty chamber of carbon nanofiber, ii. SEI is initially covered on surfaces, iii. SEI is continuously produced on the pulverized silicon and gradually fill up the empty chamber, iv. finally, SEI productions exceed the carbon chamber wall and silicon nanoparticle are no longer confined.

## Table of Contents



**Silicon nanoparticles are confined within empty chambers of polyacrylonitrile-derived carbon nanofibers.** The chambers can provide sufficient empty space to accommodate silicon volumetric expansion and retain SEI products so as to maintain the integrity of the composite structure during lithiation process. This self-supported silicon-carbon nanofiber structure exhibits high flexibility and good electrochemical performance for use as free-standing electrodes in lithium-ion batteries.